Tomographic Reconstruction of Ultrasonic Attenuation with Correction for Refractive Errors

The nonionizing and noninvasive characteristics of ultrasonics promote its increasing use in medical applications. Computerized ultrasonic attenuation tomography is one area where medically significant images may be reconstructed for diagnostic purposes. The objective of this work is to make an initial correction for refraction error and other problems present in computerized ultrasonic tomography. As a refinement of the scanning technique, our method attempts to provide high-quality projection profiles to the reconstruction algorithms. The important aspect of this new scanning mode lies in its correction for refraction in the measured attenuation profiles. In reconstructing phantom targets scanned by our experimental system, results superior to traditional line-of-sight scanning were obtained.

Introduction

In diagnostic medicine there is a growing need for an improved means of imaging internal bodily features without forced entry. These noninvasive techniques must handle a wide spectrum of medical needs ranging from imaging of the skeletal structure to investigation of the circulatory system [1, 2]. In addition, these techniques should not pose any safety problems for patients under examination [3].

The most common method of internal imaging is x-rays, which for many cases can produce clear and detailed pictures. However, its physical risk is a major concern to physicians. Its utility, moreover, is not the same for all situations. In applications where tissue differentiation of internal organ structure is desired, ultrasonic imaging techniques can provide more information without resorting to other expedients (such as injection of chemicals to enhance x-ray absorption). For general medical examinations, the nonionizing ultrasonics are considered to be less hazardous than x-rays. This safety feature combined with the capability to determine structure and differentiate between normal and pathologic tissues within the body presents motivation to improve the techniques presently being used for ultrasonic imaging [4-10].

This paper presents a new technique for measuring the projection curves required for computerized ultrasonic

attenuation tomography and experimental evaluations of this technique on simple phantoms [11, 12].

Ultrasonic imaging

As another form of radiography, diagnostic ultrasound produces a cross-sectional image of internal body structures in terms of one of the typical acoustic parameters such as reflection, attenuation, or speed of propagation [13-15]. In present medical practice, a commonly used technique is the pulse-echo mode in which the reflection of ultrasonic waves is used as the imaging parameter. From bio-acoustic studies, it has been shown that the ability to reconstruct a cross-sectional image based on attenuation or speed of propagation would provide additional significant diagnostic information for physicians [10, 16-19].

One method of measuring attenuation and speed of propagation is the transmission mode in which the transmitter and receiver are placed facing each other and scan across a cross section of the target placed between the two transducers. For each uniformly spaced point along the scan, the effect on the parameter of interest as a result of the ultrasonic wave traveling the line from transmitter to receiver is summed. The resulting shadow profile is called a projection curve (see Fig. 2, shown later). For two-dimensional cross-sectional reconstruction, the re-

Copyright 1981 by International Business Machines Corporation. Copying is permitted without payment of royalty provided that (1) each reproduction is done without alteration and (2) the *Journal* reference and IBM copyright notice are included on the first page. The title and abstract may be used without further permission in computer-based and other information-service systems. Permission to republish other excerpts should be obtained from the Editor.

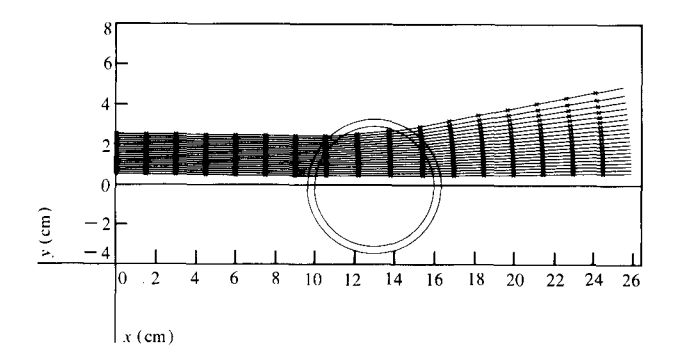


Figure 1 Effect of refraction on a parallel-ray transducer through a cylindrical target with refractive indexes of 1.6 for tube contents, 1.62 for tube, and 1.5 for outer medium.

Table 1 Acoustic properties of tissues.

Material	Characteristic impedance (g/cm ² -s × 10 ⁻⁵)	Propagation velocity (m/s)	Attenuation coefficient (dB/cm at 1 MHz)
air	0.0004	331	12
water	1.48	1480	0.0022
fat	1.38	1450	0.63
blood	1.61	1570	0.18
muscle	1.70	1585	1.8
liver	1.65	1550	0.94
kidney	1.62	1560	1.0
bone	7.80	4080	20

quired data is a set of projections taken at different angles uniformly spaced over a semicircle around the patient.

Two medically significant parameters of reconstruction are the acoustic attenuation coefficient $\alpha(\omega)$ and the velocity of propagation v of the ultrasonic wave through the medium [16, 17]. Attenuation and propagation velocity in biologic materials occur as a result of several mechanisms [17, 20, 21]. For plane sound waves at frequency ω , attenuation is defined by $\alpha(\omega)$ in the equation

$$A = A_0 e^{-\alpha(\omega)x} e^{j\omega} \left(t - \frac{kx}{\omega} \right), \tag{1}$$

where the measurement A is used to describe a sound field such as pressure, displacement, etc., A_0 is the amplitude at the origin, and k is the wave number. The combined effect of the different mechanisms on the amplitude of a wave of ultrasound traveling through the medium is characterized in terms of $\alpha(\omega)$. The acoustic attenuation for soft tissues has been found to be approximately proportional to frequency in the range of one to ten MHz.

Another parameter characteristic of the medium is the amount of time it takes for an ultrasonic wave to travel a known distance in the medium. The time-of-flight measurements result in the reconstruction of a velocity map 1/v(x, y) or the related index of refraction map n(x, y).

The reconstruction of attenuation requires accurate measurements of the sum of the ultrasonic energy elastically scattered by inhomogeneities within the tissue and the energy absorbed by the tissue by energy conversion while it is traveling designated paths through the target [22]. Any diminution of amplitude from purely geometrical effects must be removed. This means that the effects of refraction and reflection must be corrected.

In a simple interface situation, Bragg's Law tells us that the amount of refraction is dependent on the refraction indices of the two materials joining at the interface and the angle of incidence of the wave. For a material with refraction as a continuous function of spatial position, Farrell has developed a simulation program which uses ray optics for analysis [23, 24]. Rays are traced through a simulated refractive index field to the receiver plane. When a cylindrical target was used in the simulation, with the presence of all possible incident angles, the existence of a nonnegligible effect due to refraction was clearly demonstrated. In Fig. 1, refraction is greatest at those interfaces which are almost parallel to the incident beam. Each line in the beam represents a ray whose path has been traced. With the occurrence of such beam bending. traditional line-of-sight (LOS) attenuation measurements will indicate a much greater attenuation than is actually present. The reconstructions will be imperfect.

For an interface between two biological materials of characteristic impedance Z_1 and Z_2 , neglecting shear waves, it can be seen from Table 1 that reflection is small for waves with incidence perpendicular to the interface. Reflection may be quite large at nonnormal incidences [21, 25, 26].

In addition to geometric and structural problems, instrumental problems such as phase cancellation and beam width also contribute to errors in measurements. Since we are trying to measure the attenuative effects of the tissue, the other mechanisms are to be regarded as artifacts.

A typical piezoelectric receiving transducer is of finite size and produces a signal from the integral of the signal amplitude across the transducer face. Thus, if it simultaneously receives two spatially close signals 180° out of phase with respect to each other, the output will appear to be zero. This would be especially true in the presence of refraction.

Due to the existence of refraction and phase cancellation, a basic tradeoff exists in selecting the receiver diameter. To maximize the received signal in the presence of refraction, a larger receiver is more desirable. However, phase cancellation increases as the size of the receiver is increased. A smaller receiver is needed. The objective is to catch all the signal without the effects of phase cancellation.

Beam width is also an instrumental problem. Since the resolution of the system is closely dependent on the size of the beam detected, beam thickness serves to reduce the capability for differentiating small spatial changes. Like the width of the beam, beam divergence reduces the energy per unit area.

A factor relevant to both attenuation and velocity measurements is the frequency dependence of the attenuation. The frequency spectrum of the transmitted signal will change significantly after traveling through the target. Since attenuation increases with increasing frequency, the high-frequency signal components will be more attenuated than the lower-frequency parts of the signal. The received peak frequency could shift down from the initial resonant frequency of the transmitting transducer.

One method of attenuation measurement has been to measure peak amplitude without regard for frequency content. Thus, a frequency-dependent attenuation will introduce some error into this measurement. A narrow frequency spectrum would be beneficial for obtaining more accurate attenuation measurements by eliminating some of the ambiguity that a wide bandwidth would present. However, this is a direct tradeoff with phase cancellation. Having only one dominant frequency causes the signal to be highly susceptible to the distorting effects of phase cancellation. For a broad-band transducer, while certain frequencies may cancel, others will not.

In the following sections, we will present a new technique which minimizes the effects of refraction, phase cancellation and beam width divergence in transmission measurements.

Refined attenuation reconstruction

The arrangement presently used for transmission tomography has been to place the transmitter and the receiver in a line [27]. As shown in Fig. 2, the ultrasound signal is launched from the transmitter and traverses the target along path l until arrival at the receiver. The received signal amplitude can be expressed as an exponential function of the integral of α ,

$$A_{\theta}(u) = A_0 \exp\left[-\int_{l} \alpha(u, v) dv\right], \tag{2}$$

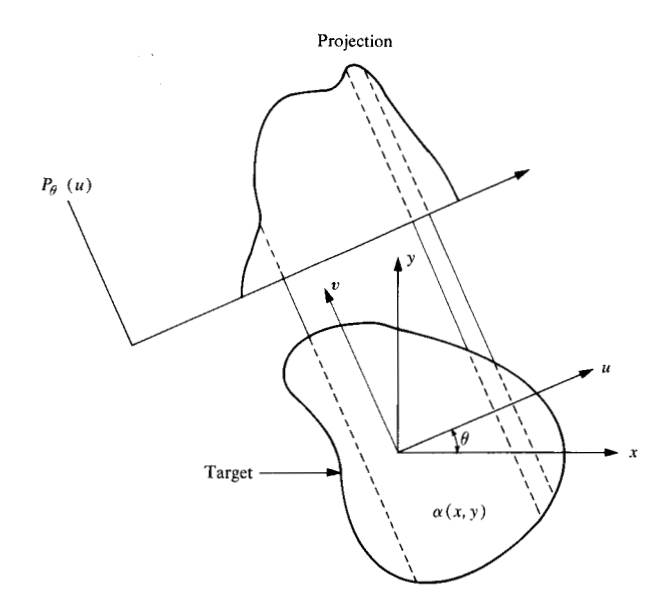


Figure 2 Projection curve geometry for parallel scanning.

where A_0 is the transmitted amplitude, θ is the viewing angle, and u, v are the Cartesian coordinates of the system. After passing through a logarithmic amplifier, the received signal is

$$\ln A_{\theta}(u) = \ln A_0 - \int_{l} \alpha(u, v) dv.$$
 (3)

A normalized attenuation projection is obtained as

$$P_{\theta}(u) = \int_{l} \alpha(u, v) dv - \int_{l} \alpha_{\mathbf{w}}(u, v) dv, \tag{4}$$

where α_w is the attenuation in the water surrounding the target. If the separation between the transducers is fixed, the second integral is a constant. The function $P_{\theta}(u)$ is then a one-dimensional projection of the change of attenuation due to the target as viewed from an angle θ . Additional projections may be measured at other angles by rotating the target after each scan. The set of projections may then be inverted by any of the several available computer algorithms developed for x-ray tomographic reconstruction [28]. This method assumes that the received signal measures the sum of attenuation along the straight line between the transmitter and the receiver. However, because of refraction and reflection, the measured attenuation may be largely due to the sensing of only a fraction of the available signal. It should also be noted that these equations do not explicitly account for the frequency dependence of attenuation. Since α is a strong function of frequency, it will cause beam softening in a pulsed signal, due to the increased absorption at higher frequencies.

73

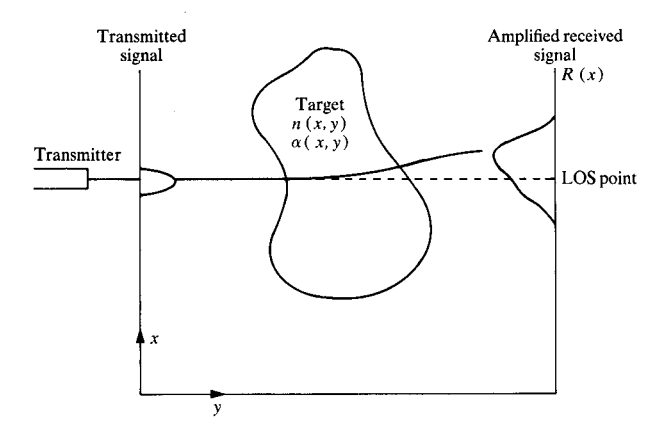


Figure 3 Beam spreading in part due to refraction.

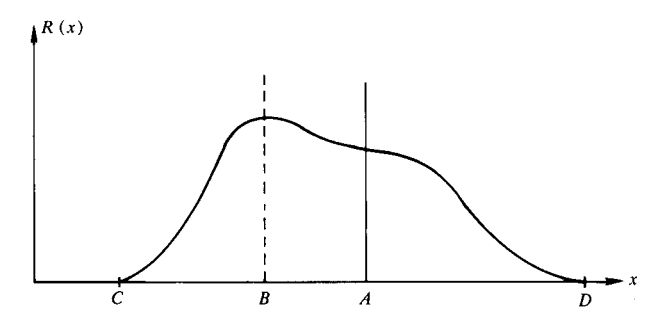


Figure 4 Traditional LOS scanning as compared to the four proposed derivations in DT scanning. R(x) is the spatial distribution of the received signal. The reconstruction parameters are:

Original, $P_{\theta}(A) = R(A)$; Peak value, $P_{\theta}(A) = R(B)$; Average value, $P_{\theta}(A) = \int_{C}^{D} R(x) dx/|D - C|$; Sum, $P_{\theta}(A) = \int_{C}^{D} R(c) dx$; Sum of squares, $P_{\theta}(A) = \int_{C}^{D} R^{2}(x) dx$.

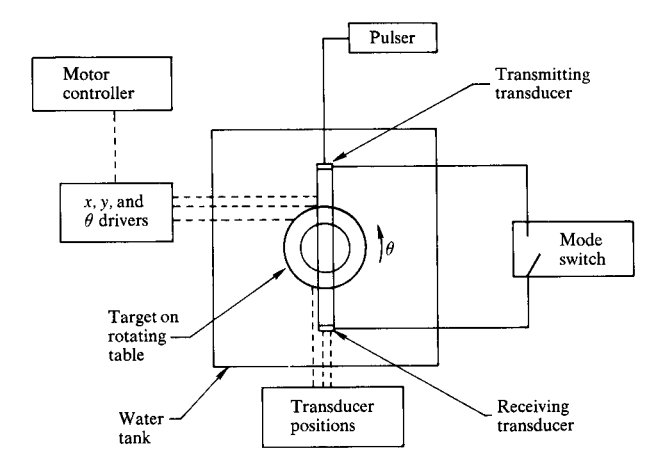


Figure 5 An implementation configuration of the LOS scanning mode.

To correct the errors in the measurements, let us consider an alternative to LOS reception. Let us scan with a small receiver some distance δx on either side of the LOS point for each transmitted point (Fig. 3). There is a received beam profile associated with each transmitter position called a miniprofile. Such a detached transmitter (DT) arrangement gives much more information about the target and has potential for corrections based on this additional knowledge.

With the DT mode of scanning, there is a whole miniprofile available where before there was only one value (LOS measurement). From each miniprofile there must be one value derived to represent the projection function at the point corresponding to the transmitter position. Four different derivations using the DT mode were investigated.

One straightforward correction is to find the maximum value of each received miniprofile. This may not be the LOS point if the target is refracting. The attenuation at this miniprofile maximum is then used as the value on the projection curve at the line-of-sight point. This correction will only be effective in the areas where the rate of change of the attenuation parameter over a distance comparable to the refraction distance is small. Otherwise, the resultant attenuation of the refracted beam and the attenuation along the straight line path beam become significantly different. If refraction is small, the path to the detected maximum point will closely approximate the straight line path to the LOS point. Thus, by accounting for beam direction changes, the refraction error will be reduced. Expected errors will be maximum near the edges of interfaces due to increased refraction and reflection.

The sum of the values in each miniprofile is another derived function to characterize the target field for each transmitter position. Although this method is similar to the integration provided by a large receiver, it will not have the instrumental phase cancellation problems of a large receiver, because each point is being summed individually.

The average of all the values in the miniprofile is similar to the sum. It more accurately handles the situation where motor fluctuations cause the number of samples in each miniprofile to vary, and thus the sum to change erroneously.

The fourth method is to sum the square of every measurement. The value used for the projection at the point corresponding to the transmitter position is the sum of the squares of each point in the miniprofile. Squaring the values on the miniprofile will cause the spatial refraction

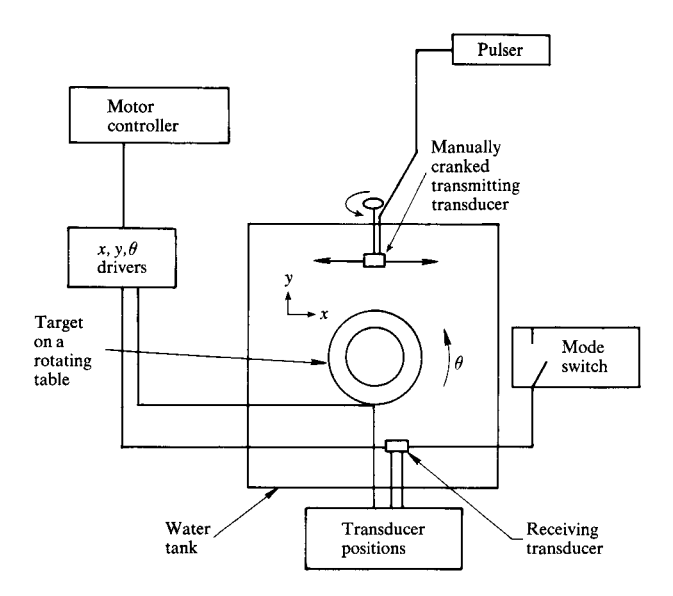


Figure 6 An implementation configuration of the DT mode of scanning.

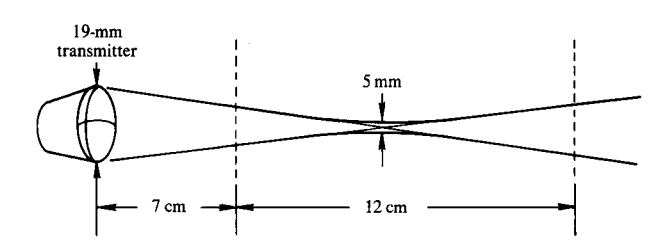


Figure 7 A focusing 2.25-MHz piezoelectric transducer.

function to become sharper and a better approximation to an impulse function. It will then be a more useful parameter to use for reconstruction.

These four alternatives to LOS scanning (see Fig. 4 for summary) were designed and implemented to correct for errors arising from refraction.

Experimental implementation

In order to acquire digitized ultrasonic data for image reconstruction, show the feasibility of the techniques discussed above, and demonstrate their potential for ultrasonic image improvement, an experimental system originally developed at the IBM Thomas J. Watson Research Center by Chow *et al.* was modified to implement these techniques [6].

The ultrasound scanning apparatus consisted basically of a water tank with two immersed transducers at opposite ends. The target sat on a rotating table between the transducer and receiver. There were two different scan-

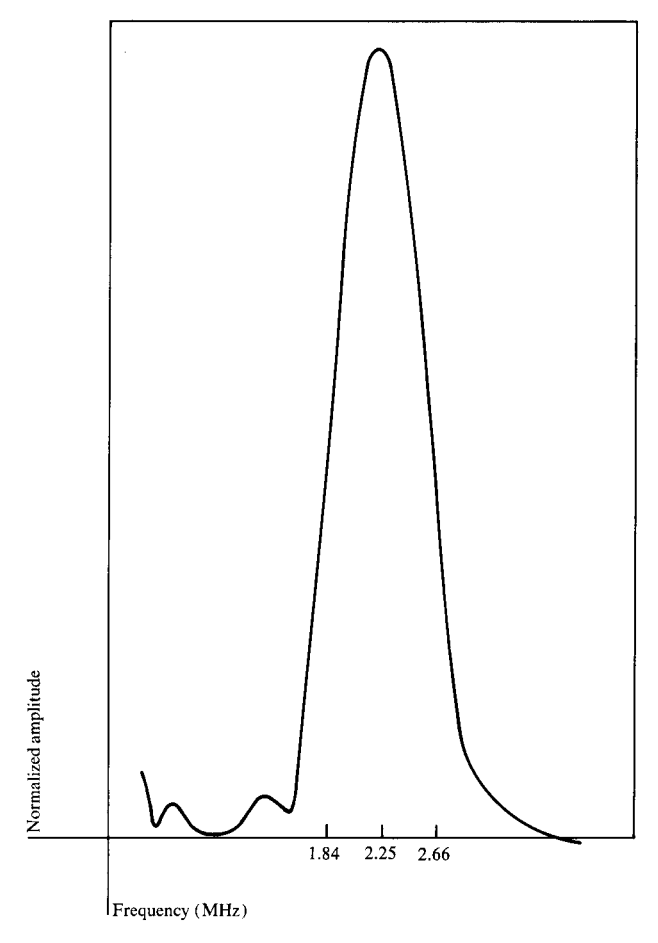


Figure 8 Frequency spectrum of transmitter signal.

ning modes of operation: 1) LOS mode (Fig. 5)—the transducers, fixed with respect to each other, were fitted into arms coaxially facing each other and moved with a computer-controlled scanning motion. 2) Detached transmitter (DT) mode (Fig. 6)—the receiver moved by computer control while the transmitter was manually cranked a uniform distance for each complete scan of the receiver. It should be pointed out that the movement of the receiver can be eliminated by an array receiver.

Measurements were taken in only one direction of scanning to avoid motor nonuniformity. Both translation and rotation motors were computer-controlled. The mechanical motor resolution was on the order of 0.012 mm in the direction of wave propagation and even better quantitatively in the direction of scanning. Angular motor resolution was also very small, on the order of 0.2 degrees. All three motor resolutions were far better than that needed for adequate fidelity. The description and basic operation of the system have been reported elsewhere [6].

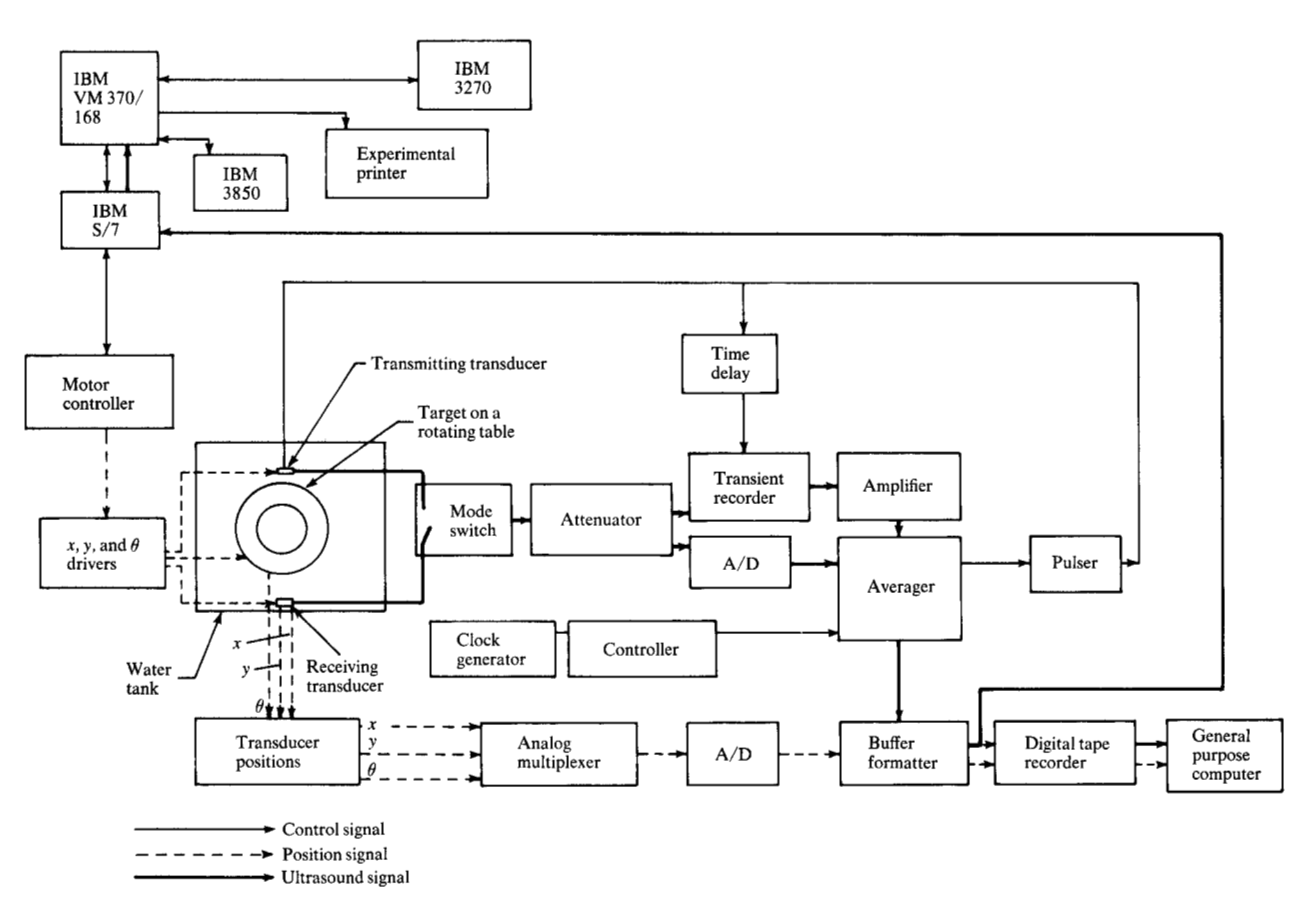


Figure 9 Block diagram of ultrasound experimental system.

The transmitter was pulsed at regular intervals and the receiver picked up the signal after transmission through the target. A focusing piezoelectric transducer with a half-power width of 5 mm was used (Fig. 7). The frequency spectrum of the transmitted signal was centered at 2.25 MHz (Fig. 8). The 12-cm-long focused region started 7 cm away from the face. Under this constraint, the distances between transmitter and receiver lines of motion for the LOS mode were approximately 16.6 cm and 18 cm for the DT mode. The receiver was a planar 2.25-MHz transducer with a face diameter of 13 mm. The scan movement was 95.25 mm in length with averaged and digitized samples spaced uniformly. An average of more than 25 kbytes of data was recorded per scan for full-wave acquisition. Due to the large amounts of data involved, when the full-wave signal was recorded (LOS or attenuation slope) the sampling interval was 0.73 mm. If only the maximum of the digitized signal was recorded (DT mode), the sampling interval was decreased to 0.18 mm. The transmitter in DT mode was cranked a total distance of 76.2 mm at 1.27-mm intervals. Each scan included portions with only water for normalization. To minimize scanning motion disturbances in the water tank, the transducers were moved at a very low speed of 3.3 mm per second. If multiangle scans were desired, the table could be rotated after each linear scan. Figure 9 shows the block diagram of the system.

Beam divergence was minimized with the use of a focusing transducer with a relatively long focal length. To minimize phase cancellation problems, the 13-mm-diameter receiver was fitted with a special purpose aperture plate, designed to receive only a small fraction of the signal while minimizing diffraction [29]. The aperture plate consists of two brass plates separated by a sealed air chamber. A 1-mm opening in the center allows signal transmission. The effect of the aperture on the received signal can be seen in Fig. 10, measured (a) with the aperture plate and (b) with no aperture. Signal strength has been decreased by 16 dB. The amount of phase cancellation is dependent on the maximum phase lag of the signals simultaneously arriving at the face of the receiver. This phase lag is a function of the ultrasound wavelength and the path length difference of those waves. If the path

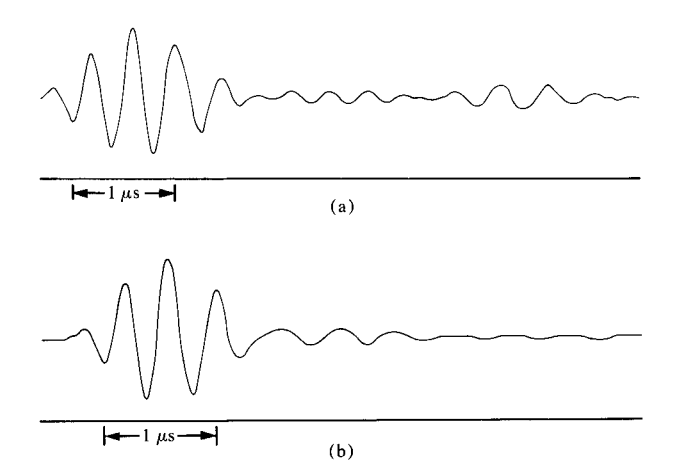


Figure 10 Received signal (a) with and (b) without aperture plate.

length difference of waves arriving within the scope of the aperture is small with respect to the wavelength, little phase cancellation will occur. In our experimental system the area of the receiver face was greatly diminished with the aperture. Actual area was decreased by a factor of $1/13^2 = 0.006$. Thus, complete cancellation does not occur. The approximation to a pinpoint receiver has been greatly improved.

Furthermore, with the use of a focusing transducer, placing the observation plane as close to the transmitter focal point as possible (Fig. 11) minimizes the amount of defocusing the signal undergoes before it is detected. This also decreases the possibility of phase cancellation at the receiver. A sample miniprofile measured on this system is shown in Fig. 12.

A phantom target composed of a cylindrical rubber tube filled with either water or castor oil was used. Castor oil was selected for testing because its acoustic characteristics are similar to those of biologic tissues. Polyethylene finger-cots filled with castor oil or water were also tested. The targets were chosen to be cylindrically symmetric because of the resulting simplification in the reconstruction computation. Theoretically, only one projection or profile of attenuation contains all the needed information for one cross-section reconstruction. In addition, a cylindrically symmetric target presents a situation where all possible incident angles are present for a range of resulting refraction errors.

With this cylindrical phantom, any error due to refraction will become more severe at interfaces parallel to the

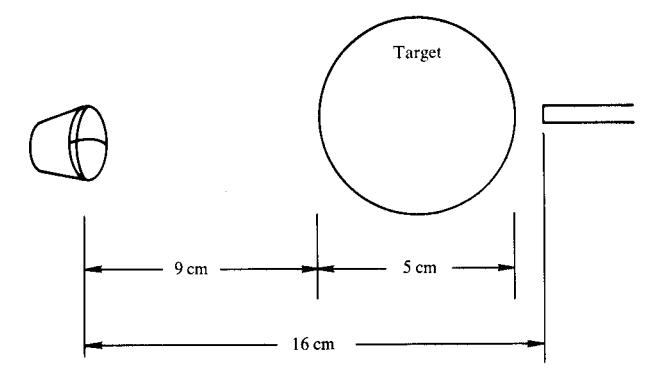


Figure 11 Target placement with respect to the transmitting and receiving transducers.

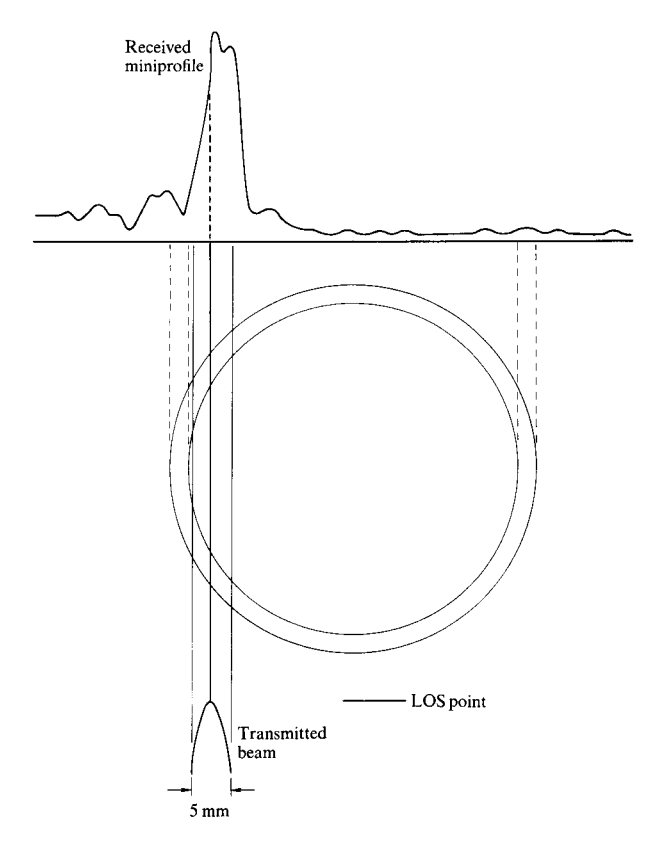


Figure 12 Measured miniprofile obtained with the DT scanning technique.

transmitted ray where the incident angle becomes large and thus the refracted angle also becomes large. At these same interfaces, reflection also becomes a problem. Beyond the critical angle the entire signal becomes a reflection. With a significant amount of reflection present, our correction for refraction would be less effective in reducing the total number of artifacts in the reconstructed



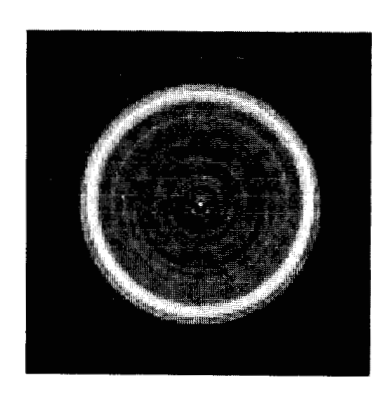


Figure 13 Reconstruction of castor oil in rubber tube with LOS scanning.

Table 2 Acoustic properties for experimental materials.

Material	Propagation velocity at 20°C (m/s)	Attenuation coefficient at 20°C (dB/cm at 2.25 MHz)
water	1480	0.0046-0.0049
castor oil	1570-1622	0.363-0.364
rubber	1900-2200	0.69-0.71

Table 3 Summary of comparison of reconstructions.

Scanning and processing mode	Oil in rubber tube	Water in rubber tube 0.19
LOS	$\gamma: 0.191$ $\xi: 0.43$	
DT	1,01-1	
peak	$\gamma: 0.10$ $\xi: 0.43-0.47$	0.07
avg	$ \gamma: 0.15 \\ \xi: 0.57-0.62 $	0.13
sum	$ \gamma : 0.13 \\ \xi : 0.57-0.62 $	0.13
sum of squares	$\gamma: 0.14 \ \xi: 0.49$	0.14
Slope of FDA	γ: 0.12-0.14 ξ: 0.27	0.18

Physical γ : 0.06 ξ : 0.51-0.52

γ : dimension ratioξ : quantitative attenuation ratio

image. However, this is practically unavoidable with a realistic target. We feel our experimental investigation is valid since less reflection can improve our results by decreasing reflection-induced errors.

It became clear during the use of the detached transmitter arrangement that refraction is a major problem with ultrasonic transmission. The receiver detected a signal over a distance which was more than 2.5 times the size of a beam received in water. Spreading of this magnitude is due to beam divergence, target refraction, and reflection.

Experimental results

Using the proposed detached transmitter technique outlined in the previous sections, significant improvements over LOS attenuation reconstructions were observed.

Two criteria were used for comparison: 1) The ratio of tube thickness to the cylinder inner radius in the reconstructed images was calculated. For the actual target, this ratio is

$$\gamma = \frac{\text{tube thickness}}{\text{cylinder radius}} = 0.06. \tag{5}$$

2) Each method was also evaluated with respect to the experimentally determined quantitative values of attenuation. Define ξ as the ratio of average castor oil attenuation to rubber attenuation with respect to water

$$\xi = \frac{\bar{\alpha}_{\text{castor oil}} - \bar{\alpha}_{\text{water}}}{\alpha_{\text{rubber}} - \bar{\alpha}_{\text{water}}}$$
 (6)

Here the average attenuation values for castor oil and water are derived from a midline slice of the resultant image. The rubber cylinder was not thick enough to allow for an average to be taken. Instead, the value for rubber attenuation was taken to be the peak of the derived attenuation midline. Using the experimentally determined values in Table 2 for the materials included in this study, ξ has a range of 0.511-0.522.

As seen in Table 3, the peak of the miniprofile results in the best reconstructed images. This technique would seem to be the most viable of the methods investigated. A discussion of the results follows.

Figure 13 shows the reconstructed image of a target of rubber cylinder filled with castor oil scanned with aperture in the traditional LOS mode. Shapes are shadowy and the jitter indicates the presence of considerable error. In addition to this error, blurring has increased the ratio of tube thickness to inner radius γ from 0.06 to 0.191, a substantial error. Quantitatively, the ratio of average value of attenuations of castor oil to rubber $\xi = 0.428$,

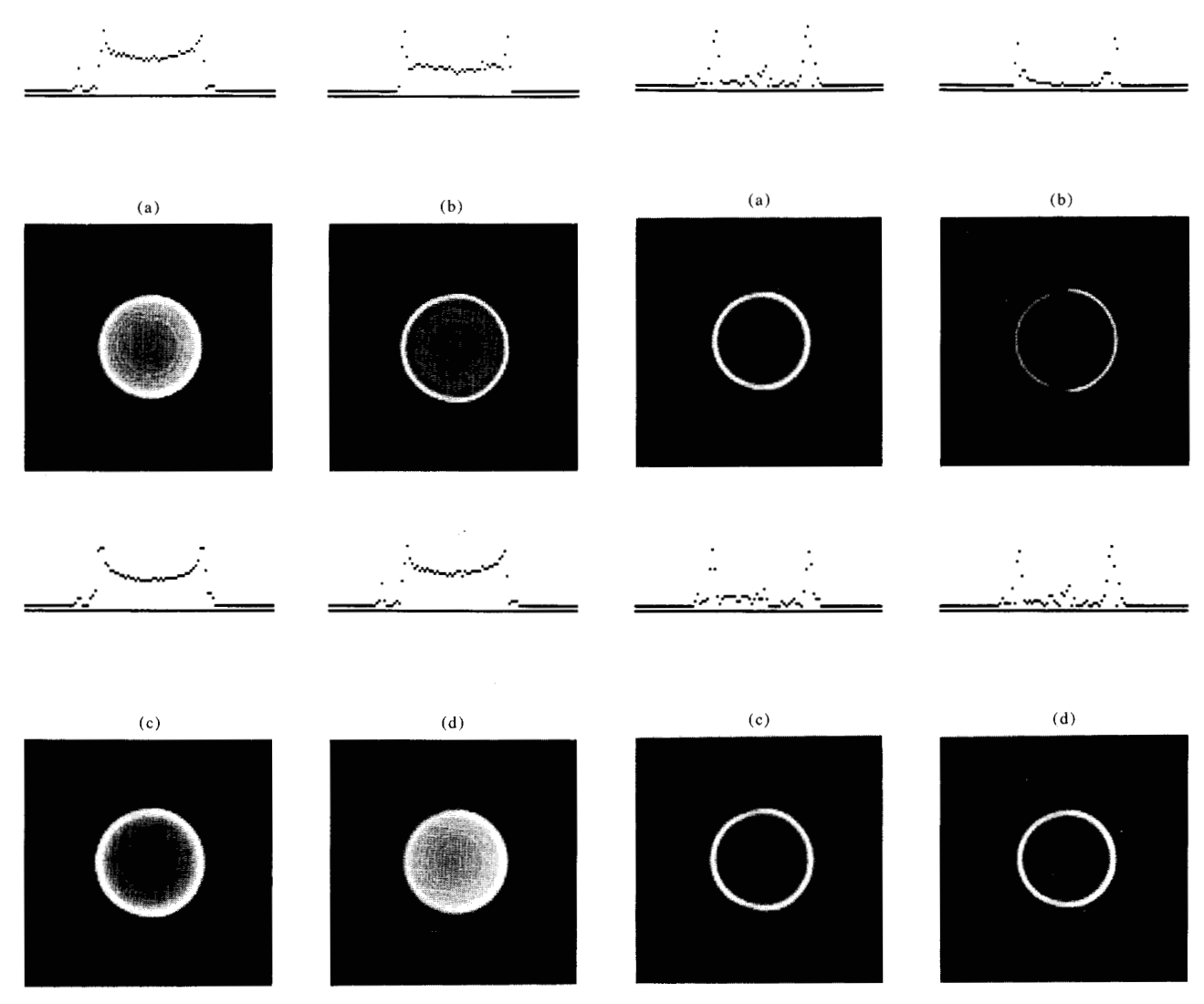


Figure 14 Reconstruction of castor oil in rubber tube with DT scanning. (a) sum of miniprofile, (b) peak of miniprofile, (c) sum of squares of miniprofile, (d) average of miniprofile.

Figure 15 Reconstruction of water in rubber tube with DT scanning. (a) sum of miniprofile, (b) peak of miniprofile, (c) sum of squares of miniprofile, (d) average of miniprofile.

decreased from 0.511. The same technique for a cylindrical tube filled with water showed similar results.

For a castor oil target, the reconstruction based on the peak detected in the DT mode resulted in a much sharper and clearer image [Fig. 14(b)]. Though there are errors at the sharp interfaces, they were only obvious in the immediate vicinity of the interface. The ratio of thickness to radius γ is 0.102 for the castor oil target. Quantitatively, the values of rubber and castor oil with respect to water ξ lie in the range 0.432-0.470. Miniprofile peak for a water-filled tube in DT mode improved the γ to 0.069 [Fig.

15(b)]. In addition, the water value within the tube is much more uniform. The fluctuations present in the LOS method have been reduced.

Reconstruction with the average value of the miniprofile as the parameter resulted in an image with improved characteristics of sharpness and clarity. The improvement is similar to but less than that exhibited by peak reconstruction [see Fig. 14(d) for castor oil target]. Here the quantitative values show a ξ of 0.567-0.617. Dimensional ratio is $\gamma = 0.146$. As opposed to the peak reconstruction which resulted in a very clean image, recon-

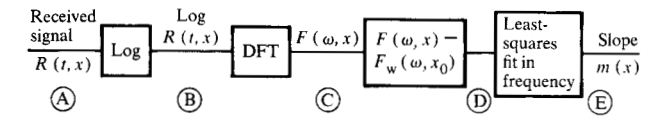


Figure 16 Block diagram of frequency-dependent attenuation reconstruction method. $F_{\rm w}(\omega, x_0)$ is the average of four Fourier transforms of water signals. Note that frequency-dependent attenuation measurements are taken in the line-of-sight mode.

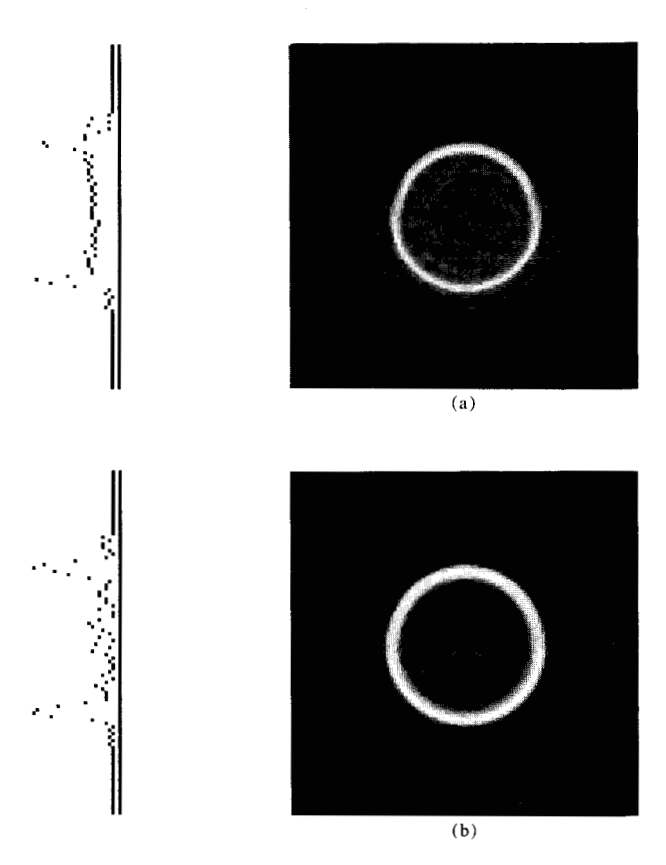


Figure 17 Reconstruction of the slope of the frequency-dependent attenuation curve: (a) castor oil target, (b) water target.

struction of the miniprofile average produced a superfluous ring around the target. This artifact may be due to reflection effects at the edge of the tube. Such reflection will be included in the averaging method. The asymmetry of the extraneous effects ring is due to an alignment problem in the placement of the two transducers facing each other. Again for a water target [Fig. 15(d)], the average of the miniprofile does not seem as effective as the peak in improving the quality of the image. Improvement of the γ

was changed from the LOS value of 0.185 to 0.132. Moreover, the extraneous ring was also introduced around the outer surface of the cylinder.

As the sum of the values in the miniprofile is very similar to the average value, the resulting images are also similar [see Fig. 14(a) for the castor oil target] with $\gamma = 0.130$ and $\xi = 0.567$ -0.617. In the case of a water target [Fig. 15(a)], the sum produced a $\gamma = 0.132$ similar to the value for the average of the miniprofile. The extraneous ring was also present. The uniformity of the water values within the cylinder continues to be an improvement over the LOS mode.

The sum of squares is in effect a sum of the spatial power spectrum of the transmitted signal in the cross-sectional plane. Used as a reconstruction parameter it also gave good clear images [Fig. 14(c)]. $\gamma = 0.143$ is the ratio of dimensions and quantitatively $\xi = 0.485$. For a water target [Fig. 15(c)], the sum of squares of the miniprofile seemed to produce slightly more ringing than peak, sum, or average. Though an improvement over LOS traditional preprocessing, the γ was only improved to 0.144.

All the DT mode reconstructions produced good sharp images. The prevalence of jitter was greatly decreased. This was due largely to the correction for refraction since efforts to minimize phase cancellation and beam width divergence were made for both the LOS and DT modes. The peak of the miniprofile seems obviously the best choice of the four deriving functions considered here.

For comparison purposes, frequency-dependent attenuation was also taken via the LOS mode. A block diagram of the processing steps is shown in Fig. 16. Each signal was normalized with a water signal in the frequency domain. Then a least-squares line was fitted through the points in the frequency spectrum of each signal corresponding to a range around the resonant frequency of the transducer [30]. This derived slope was used as the value of the profile at the LOS point [31]. Note that the bandwidth over which the slope measurements were derived was 800 kHz, which is quite narrow compared to what others have used. Consequently, our estimates of $\partial \alpha/\partial \omega$ may be more susceptible to numerical errors.

Experimentally, reconstructions of the slope of the attenuation vs frequency curve seemed to do, at best, as well as the peak of the miniprofile. The resultant dimension ratio for a castor oil target [Fig. 17(a)] was $\gamma = 0.105$ -0.140. Less ringing was present than with LOS traditional scanning, but most of the DT modes with castor oil targets did considerably better. Here it could not be determined whether the reconstruction was quantitatively correct

since the $\partial \alpha/\partial \omega$ was not known for all the materials used. Nevertheless, for a castor oil target, the quantitative ratio \mathcal{E} is 0.265.

For a water target, however, the slope of the attenuation vs frequency curve performed considerably worse with a $\gamma = 0.175$ [Fig. 17(b)]. This method seemed to perform better where there were less sharp changes in attenuation (i.e., water targets over castor oil targets). Though the resolution is poorer than the miniprofile peak, the slope of attenuation with respect to frequency does not produce some of the extraneous outer rings that the DT modes other than miniprofile peak seemed to introduce.

Though the slope of the frequency-dependent attenuation (FDA) methods performed less capably than the miniprofile peak of the DT mode, they seemed to do better than the LOS attenuation reconstructions.

With a Gaussian assumption on the point spread function of the transducers, beam deconvolution was applied to the measured profile. The resultant reconstructed images showed little improvement. Several types of low-pass filtering were applied to the reconstructed images to smooth out the ringing in the images. The improvements were found to be relatively small. A plausible explanation is that artifacts arising from refraction require a more direct correction than postprocessing filtering alone.

Concluding remarks

Computerized ultrasonic attenuation tomography involves reconstruction of ultrasonic attenuation incurred by a wave traveling through the medium. Measured attenuation contains the effects of energy absorption along with other mechanisms such as refraction, reflection, and instrumental performance. In this study, a technique of making corrections for errors due to refraction and phase cancellation in the attenuation measurements was investigated. For a set of simple phantom targets, the proposed alternatives to the conventional LOS attenuation measurements resulted in improved attenuation reconstruction. Compared with the reconstruction of $\partial \alpha / \partial \omega$ of those targets, our method also appeared to be superior. Further evaluation of the proposed DT mode would include the investigation of the effect of reflection errors and the development of techniques to reduce artifacts arising from reflection errors.

Acknowledgments

We are grateful to Ed Farrell for discussions on his work on ray-tracing simulations which contributed to the progress of this work. We thank C. K. Chow for his enthusiastic support and useful discussions. We welcome the opportunity to thank Robert J. Von Gutfeld for his discussions and also for providing us with the aperture used in the scanning system. The programming assistance of Alan Stern and the mechanical engineering design of George Forchi are much appreciated, and we acknowledge the helpful comments from the reviewers.

References

- M. G. Maginness, "Methods and Terminology for Diagnostic Ultrasound Imaging Systems," Proc. IEEE 67, 641-653 (1979).
- T. L. Rhyne, "Acoustic Instrumentation and Characterization of Lung Tissue," Ultrasound in Biomedicine Series, Vol. 2, D. N. White, Ed., Research Studies Press, Forest Grove, OR, 1977.
- F. J. Fry, "Biological Effects of Ultrasound—A Review," Proc. IEEE 67, 604-619 (1979).
- P. L. Carson, D. E. Dick, G. A. Thieme, M. L. Dick, E. J. Bayly, T. V. Oughton, G. L. Dubuque, and H. P. Bay, "Initial Investigation of Computed Tomography for Breast Imaging with Focused Ultrasound Beams," *Ultrasound in Medicine* 4, 319-322 (1978).
- P. L. Carson, T. V. Oughton, W. R. Hendee, and A. S. Ahuja, "Imaging Soft Tissue Through Bone with Ultrasound Transmission Tomography by Reconstruction," *Med. Phys.* 4, 302-309 (1977).
- C. K. Chow, S. S. Wang, T. Kaneko, and T. Perry, "An Experimental Data Acquisition System for Ultrasound Imaging," *IEEE Trans. Instrum. Meas.* IM-28, 79-83 (1979).
- G. H. Glover, "Computerized Time-of-Flight Ultrasonic Tomography for Breast Examination," Ultras. Med. Biol. 3, 117-127 (1977).
- 8. G. L. Gooberman, *Ultrasonics: Theory and Application*, Hart Publishing Co., Inc., New York, 1968, pp. 113-127.
- C. V. Jakowatz, Jr. and A. C. Kak, "Computerized Tomographic Imaging Using X-Rays and Ultrasound," *Technical Report EE* 76-26, School of Electrical Engineering, Purdue University, Lafayette, IN, 1976.
- P. P. Lele, A. B. Mansfield, A. I. Murphy, J. Namery, and N. Senapati, "Tissue Characterization by Ultrasonic Frequency-Dependent Attenuation and Scattering," Proceedings of Seminar on Ultrasonic Tissue Characterization (M. Linzer, Ed.), National Bureau of Standards, Gaithersburg, MD, May 28-30, 1975, pp. 167-196.
- K. M. Pan, "Computerized Ultrasonic Attenuation Tomography with Refraction Corrections," MS Thesis, Massachusetts Institute of Technology, Cambridge, MA, 1979.
- 12. K. M. Pan and C. N. Liu, "Computerized Ultrasonic Attenuation Tomography with Refraction Corrections," Proc. 4th International Symposium on Ultrasonic Imaging and Tissue Characterization, National Bureau of Standards, Gaithersburg, MD, June, 1979 (abstract).
- J. F. Havlice and J. C. Taenzer, "Medical Ultrasonic Imaging: An Overview of Principles and Instrumentation," Proc. IEEE 67, 620-641 (1979).
- J. Jellins and G. Kossoff, "Velocity Compensation in Water-Coupled Breast Echography," *Ultrasonics* 11, 223-226 (1973).
- C. R. Meyer, "An Iterative, Real-Time Method of Estimating Biological Tissue Absorption Coefficients IN VIVO Using Pulse-Echo Ultrasound," IEEE Ultrasonics Symposium Proceedings, 1977, IEEE Cat. No. 77CH1264-1SU, pp. 198-201.
- F. Dunn, "Ultrasonic Attenuation, Absorption, and Velocity in Tissues and Organs," Proceedings of Seminar on Ultrasonic Tissue Characterization (M. Linzer, Ed.), National Bureau of Standards, Gaithersburg, MD, May 28-30, 1975, pp. 28-30.
- 17. I. E. El'piner, Ultrasound: Physical, Chemical, and Biological Effects, authorized translation from the Russian by F. L. Sinclair Consultants Bureau, New York, 1964.

81

- 18. J. G. Miller, D. E. Yuhas, J. W. Mimbs, S. B. Dierher, L. J. Busse, J. J. Laterra, A. N. Weiss, and B. E. Sobel, "Ultrasonic Tissue Characterization: Correlation Between Biochemical and Ultrasonic Indices of Myocardial Injury," *IEEE Ultrasonics Symposium Proceedings*, 1976, IEEE Cat. No. CH1120-5SU, pp. 33-43.
- "Recent Advances in Ultrasound In Biomedicine," Ultrasound in Biomedicine Series, Vol. 3, D. N. White, Ed., Research Studies Press, Forest Grove, OR, 1977.
- W. J. Fry, "Mechanism of Acoustic Absorption in Tissue," Acoust. Soc. America 24, 412-415 (1952).
- 21. P. N. T. Wells, *Physical Principles of Ultrasonic Diagnosis*, Academic Press, London, 1969.
- C. R. Hill and R. J. Parry, "Ultrasonic Velocity and Attenuation in Mammalian Tissues," J. Acoust. Soc. America 63, 940-953 (1978).
- 23. E. J. Farrell, "Processing Limitations of Ultrasonic Image Reconstruction," Proceedings of IEEE Computer Society Conference on Pattern Recognition and Image Processing, June 1978, IEEE Cat. No. 78CH1318-5C, pp. 8-15.
- 24. E. J. Farrell, "Tomographic Image Correction with Simulation," *IBM Tech. Disclosure Bull.* 22, 3456 (1980).
- D. E. Goldman and T. F. Hueter, "Tabular Data of the Velocity and Absorption of High-Frequency Sound in Mammalian Tissues," J. Acoust. Soc. America 28, 35-37 (1956) [Errata: J. Acoust. Soc. America 29, 655 (1957)].
- G. D. Ludwig, "The Velocity of Sound Through Tissues and the Acoustic Impedance of Tissues," J. Acoust. Soc. America 22, 862-866 (1950).
- 27. J. F. Greenleaf and S. A. Johnson, "Algebraic Reconstruction of Spatial Distributions of Refractive Index and Attenuation in Tissues from Time-of-Flight and Amplitude Pro-

- files," Proceedings of Seminar on Ultrasonic Tissue Characterization (M. Linzer, Ed.), National Bureau of Standards, Gaithersburg, MD, May 28-30, 1975, pp. 109-119.
- R. Gordon and S. A. Johnson, "Three-Dimensional Reconstruction from Projections: A Review of Algorithms," *Intl. Rev. Cytology* 38, 111-151 (1974).
- R. Von Gutfeld, "Special Aperture Plate for Ultrasonic Imaging Resolution," *IBM Tech. Disclosure Bull.* 21, 3864–3856 (1979).
- A. C. Kak and K. A. Dines, "Signal Processing of Broadband Pulsed Ultrasound: Measurement of Attenuation of Soft Biological Tissues," *IEEE Trans. Biomed. Eng.* BME-25, 321-344 (1978).
- J. R. Klepper, G. H. Brandenburger, L. J. Busse, and J. G. Miller, "Phase Cancellation, Reflection, and Refraction Effects in Quantitative Ultrasonic Attenuation Tomography," *IEEE Ultrasonics Symposium Proceedings*, 1977, IEEE Cat. No. 77CH1264-1SU, pp. 182-188.

Received December 17, 1979; revised August 11, 1980

Ms. Kelly M. Pan is located at the Harvard Business School, Boston, Massachusetts; C. N. Liu is located at the IBM Thomas J. Watson Research Center, Yorktown Heights, New York 10598.